


## Effects of collectively induced scattering of gas stream by impurity ensembles: Shock-wave enhancement and disorder-stimulated nonlinear screening

O. V. Kliushnychenko\* and S. P. Lukyanets†

*Institute of Physics, NAS of Ukraine, Prospect Nauky 46, 03028 Kiev, Ukraine*

 (Received 16 September 2017; revised manuscript received 14 July 2018; published 6 August 2018)

We report on specific effects of collective scattering for a cloud of heavy impurities exposed to a gas stream. Formation is presented of a common density perturbation and shock waves, both generated collectively by a system of scatterers at sudden application of the stream-inducing external field. Our results demonstrate that (i) the scattering of gas stream can be essentially amplified, due to nonlinear collective effects, upon fragmentation of a solid obstacle into a cluster of impurities (heterogeneously fractured obstacle); (ii) a cluster of disordered impurities can produce considerably stronger scattering accompanied by enhanced and accelerated shock wave, as compared to a regularly ordered cluster. We also show that the final steady-state density distribution is formed as a residual perturbation left after the shock front passage. In particular, a kinklike steady distribution profile can be formed as a result of shock front stopping effect. The possibility of the onset of solitary diffusive density waves, reminiscent of precursor solitons, is shown and briefly discussed.

DOI: [10.1103/PhysRevE.98.020101](https://doi.org/10.1103/PhysRevE.98.020101)

*Introduction.* Gas stream scattering by an impurity cloud often leads to pronounced collective effects. This can be manifested by the formation of a common perturbation “coat” around a cloud of scatterers or common wake, localization of gas particles (blockade effects), induced correlations, and formation of nonequilibrium (dissipative) structures in the ensemble of impurities. These types of phenomena are intrinsic in various physical systems, including examples from hydrodynamics [1,2], dusty plasmas [3], quantum liquids, or Bose condensates [4,5], and can exhibit unusual behavior such as non-Newtonian wake-mediated forces [3,6–12], which is characteristic of diffusive or dissipative systems. Spatiotemporal characteristics of medium perturbations are mostly determined by the mechanism of energy losses specific to each particular system and by the properties of the medium itself, e.g., nonlinearity of associated field.

A steady-state wake profile, induced by impurities under gas flow scattering, can be considered as a residual perturbation of gas density established after its evolution over a long time. However, the properties and behavior of the system during its transit to the steady regime can significantly differ from those at steady state. For example, under abrupt activation of gas or liquid flow (or sudden impurity displacement), the formation of a wake around impurities can be accompanied by propagation of a shock wave and sign change of correlation function or dissipative force between impurities [13–15].

In this Rapid Communication, we consider the properties of nonequilibrium formations resulting from scattering of the gas stream by a cloud of impurities and examine the role of collective effects, with particular attention to the formation dynamics of common impurity wake (density perturbation “coat”) in the case when the stream-inducing driving field is

applied suddenly (nonadiabatically). Specifically, we analyze the properties of spatiotemporal evolution of shock waves generated collectively by a system of scatterers. We examine the effects of the inner structure of impurity clusters, total drag (friction) force, and possible shock-wave enhancement due to collective scattering accompanied by the nonlinear blockade effect in a gas. Note that scattering of driven gas particles was addressed earlier (e.g., [16]) mostly for uniform (on average) distribution of impurities throughout the entire system and in first order of the impurity density (typically  $\sim 10^{-3}$ ). Here, we consider the stream scattering on relatively dense ( $\gtrsim 10^{-1}$ ) and spatially finite clouds (clusters) of impurities.

We focus on a purely dissipative (diffusive) system and make use of the minimal classical two-component lattice gas model with hard-core repulsion; that is, each lattice site can be occupied by only one particle. Despite the short range of interparticle interaction it was shown to give rise to peculiar nonlinear effects essentially manifested at high gas concentrations. These are the dissipative pairing effects [8,17], the wake inversion and switching of wake-mediated interaction [8,18], formation of nonequilibrium structures [19–22], etc. As will be shown, the nonlinear effects considerably affect collective scattering.

The kinetics of a two-component lattice gas is described by the standard continuity equation (see, e.g., [23,24]),  $\dot{n}_i^\alpha = \sum_j (J_{ji}^\alpha - J_{ij}^\alpha) + \delta J_i^\alpha$ , where  $\alpha = 1, 2$  labels the particle species and  $n_i^\alpha = 0, 1$  are the local occupation numbers of particles at the  $i$ th site.  $J_{ij}^\alpha = v_{ij}^\alpha n_i^\alpha (1 - \sum_\beta n_j^\beta)$  gives the average number of jumps from site  $i$  to a neighboring site  $j$  per time interval,  $v_{ij}^\alpha$  is the mean frequency of these jumps. In what follows, fluctuations of the number of jumps [24] (the term  $\delta J_i^\alpha$ ) are neglected. To describe the scattering of a particle stream by an impurity cloud, we assume (see Refs. [8,18]) that one of the two components  $u_i = 0, 1$  describes the given distribution of impurities and is static ( $v_{ij}^1 \equiv 0$ ), while another one  $n_i(t)$  is mobile. The presence of a weak driving field

\*kliushnychenko@iop.kiev.ua

†lukyan@iop.kiev.ua

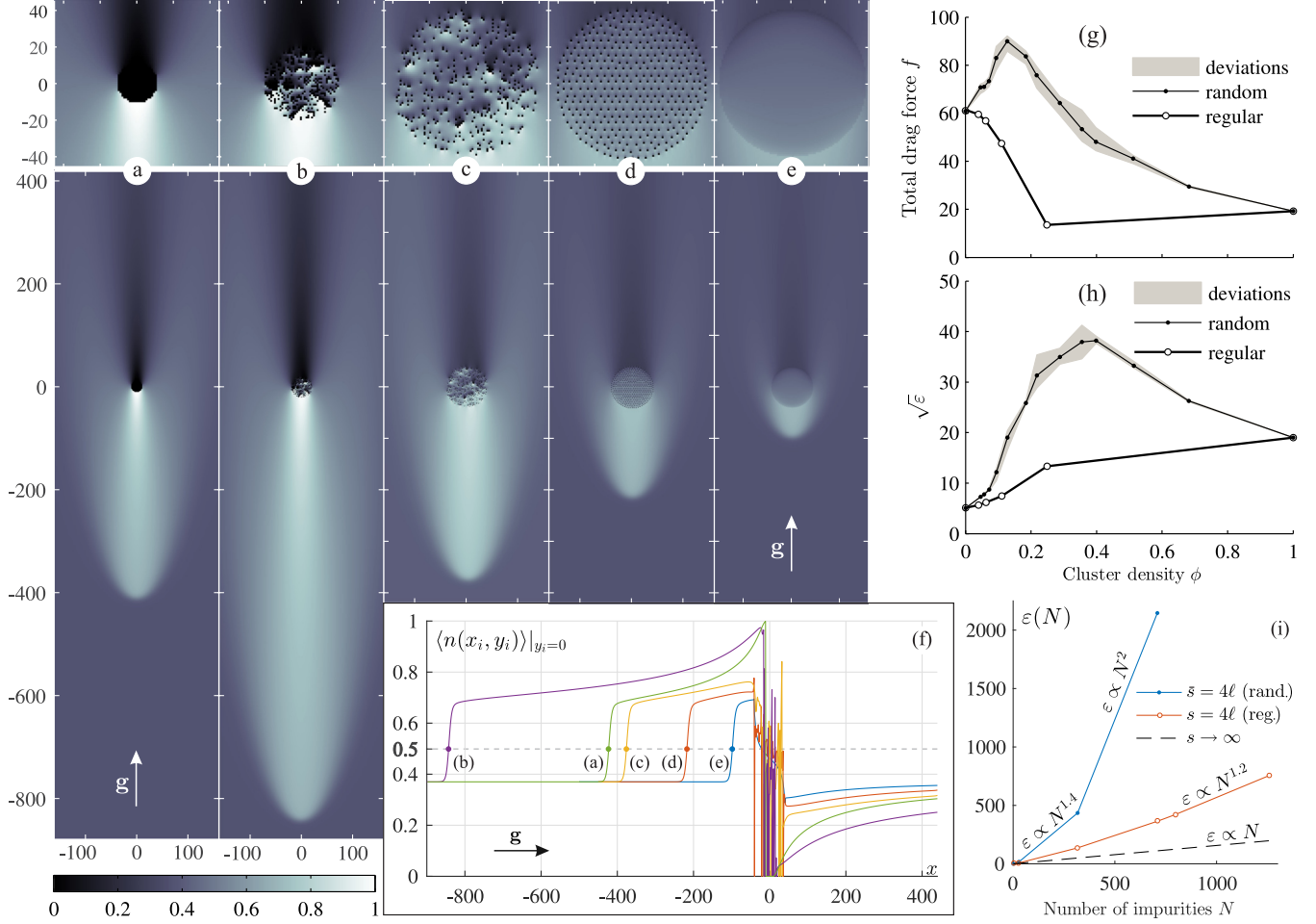


FIG. 1. Enhancement of scattering intensity. Steady-state distributions of mean concentration  $\langle n(x_i, y_i) \rangle$  [panels (a)–(e)] illustrate enhanced scattering (blockade region growth) for a heterogeneously fractured obstacle introduced by collective behavior. A close view of the impurity cluster inner structure for each case is shown at the top: (a) solid obstacle, (b) and (c) random clusters, (d) regular cluster, (e) uniform cluster.  $R = 10.8\ell$  for (a),  $R = 20\ell$  for (b), and  $R = 40\ell$  for (c)–(e). Number of constituent single-site impurities is  $N = 362$ ,  $n_0 = 0.37$ ,  $|\mathbf{g}| = 0.5$  (stream is directed along the  $x$  axis) for all calculated distributions. Corresponding density profiles  $\langle n(x_i, y_i) \rangle|_{y_i=0}$  are presented in panel (f). Plots (g) and (h) show the dependencies of total drag force  $f \equiv |f|$  (units of  $kT/\ell$ ) and  $\sqrt{\varepsilon}$  on cluster density  $\phi$ ;  $R \in (\infty, 10.8]$ ,  $N = 362$ ,  $n_0 = 0.2$ . Plot (i) shows the dependence of dispersion  $\varepsilon$  on impurity number  $N$  at  $n_0 = 0.3$ ;  $\bar{s}$  (or  $s$ ) stands for the (mean) distance between impurities;  $s = 4\ell$  corresponds to cluster density of  $\phi = 0.06$ .

(force)  $\mathbf{G}$ ,  $|\mathbf{g}| = \ell|\mathbf{G}|/(2kT) < 1$  ( $\ell$  is the lattice constant), leads to asymmetry of particle jumps for the mobile component:  $v_{ji} \approx v[1 + \mathbf{g} \cdot (\mathbf{r}_i - \mathbf{r}_j)/\ell]$ . As in [22,25,26], we use the mean-field approximation,  $\partial_t \langle n_i \rangle = \sum_j (\langle J_{ji} \rangle - \langle J_{ij} \rangle)$ ,  $\langle J_{ji} \rangle = v_{ji} \langle n_j \rangle (1 - \langle n_j \rangle - u_i)$ , where  $\langle n_i \rangle = \langle n(\mathbf{r}_i) \rangle \in [0, 1]$  describes the mean occupation numbers at sites  $\mathbf{r}_i$  or the density distribution of flowing gas particles,  $n_0 \equiv n(|\mathbf{r}| \rightarrow \infty)$  being the equilibrium gas concentration (bath fraction). In what follows, we consider the two-dimensional (2D) case.

*Collective scattering effects.* We start by outlining the two basic effects readily seen from Figs. 1(a)–1(e). Panels (a)–(c) represent the nonequilibrium steady-state density distribution  $\langle n(\mathbf{r}_i) \rangle$  produced under scattering of streaming gas particles on the collection of point impurities arranged into the compact impermeable obstacle, dense impurity cluster (fractured obstacle), and sparse cluster, all of which consist of the same number of impurities  $N$ . The qualitative differences in scattered field

$\delta n(\mathbf{r}_i) = \langle n(\mathbf{r}_i) \rangle - n_0$  constitute the essence of the first effect: Fragmentation of a solid obstacle into a cluster of separate impurities can enhance the gas stream scattering. This effect results from the collective blockade effect [8,18] which leads to screening of the gas stream between impurities. For impurity cluster density  $\phi = N/\pi R^2 < 1$  ( $R$  is the cluster radius), as Fig. 1(b) suggests, the blockade region is considerably larger than for a compact (solid) cluster [ $\phi = 1$ , Figs. 1(a) and 1(f)] as well as a diluted one,  $\phi \ll 1$ .

The second effect consists in enhancement of scattering that is provoked by the inhomogeneity of impurity distribution within a cluster [Figs 1(c)–1(e) and 1(f)]. This effect is analogous to that of light scattering on inhomogeneities in distribution of atoms (dipole moments) that is determined by the fluctuation of their number density in a definite volume or by the two-point correlation function [27–31]. As seen from Figs 1(c)–1(e), the scattering is less efficient for a regularly ordered cluster. Note that a disordered cluster can

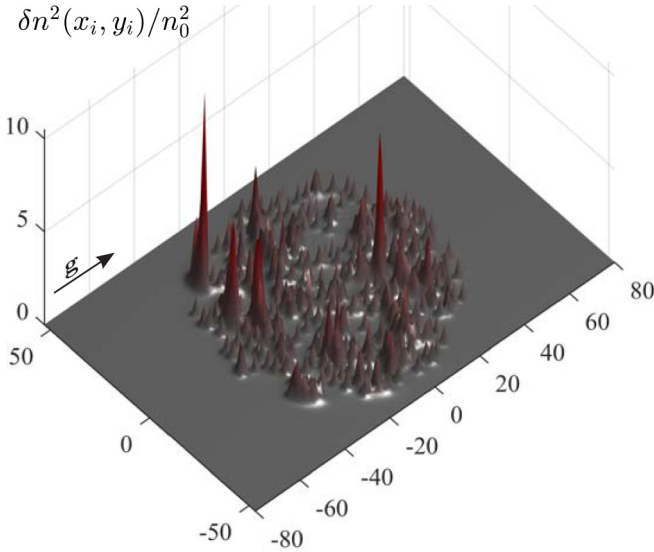


FIG. 2. Strong local fluctuations of scattered field  $\delta n(x_i, y_i)$  inside a random impurity cluster.  $\phi = 0.0569$  ( $N = 362$ ,  $R = 45\ell$ ),  $n_0 = 0.2$ ,  $|\mathbf{g}| = 0.5$ .

provoke strong local fluctuations of scattered field  $\delta n(\mathbf{r})$  inside a cluster<sup>1</sup> (see Fig. 2), i.e.,  $\delta n^2(\mathbf{r}_i) > n_0^2$ . This means that the problem of gas stream scattering on such a structure cannot be adequately described by introducing the effective diffusion coefficient for a cluster or its penetration index [18] [Figs. 1(c)–1(f)]. In addition, this can lead to high-magnitude local fluctuations of induced dissipative interaction between impurities.<sup>2</sup>

The magnitude of scattered field  $\delta n(\mathbf{r})$  can be characterized by a quantity like total density dispersion  $\varepsilon \equiv \overline{\delta n^2} \propto \int \delta n^2(\mathbf{r}) d\mathbf{r}$ . For the cluster of  $N$  infinitely distant (independent) impurities, i.e., when their mean separation length  $\bar{s} \rightarrow \infty$ , the dispersion is simply  $\varepsilon \approx \sum_{i=1}^N \overline{\delta n_i^2} \approx N \overline{\delta n_*^2} \propto N$ , where  $\overline{\delta n_*^2}$  is dispersion for a single impurity. Figure 1(i) shows that dependence  $\varepsilon(N)$  for the impurity cluster can become power law and, in particular, for the random cluster is  $\propto N^2$ , which signifies the intrinsically collective scattering.

The total drag force<sup>3</sup> acting on the impurity cluster also turns out to be quite sensitive to its density  $\phi$  and cluster inner structure. As Fig. 1(g) suggests, the behavior is qualitatively different for random and regular clusters. At early stages of confluence,  $\phi \ll 1$ , when collective wake-mediated interactions come into play, the regular cluster tends to reduce the total drag force exerted by the gas particles [Fig. 1(g)]. Conversely, the random cluster tends to increase the drag

force until the common blockade region ahead of impurities is formed. The latter screens the impurity cluster as a whole from streaming gas particles, thereby reducing the drag force. This transformation of a common perturbation “coat” is reflected in the enhancement peak of the total drag force exerted on the extended inhomogeneous cluster [see Fig. 1(g)]. Upon further increase of cluster density, the blockade region takes a more advantageous streamlined shape, such as that shown, e.g., in Figs. 1(c) or 1(b). That also contributes toward drag force decrease until the value at  $\phi = 1$  (solid obstacle) is reached [Fig. 1(g)]. At the same time, the dependence of  $\sqrt{\varepsilon}$  on random-cluster density  $\phi$  has a characteristic enhancement peak which is absent for a regular cluster, as shown in Fig. 1(h). Thus, collective gas scattering compounded by nonlinear effects can exhibit a qualitatively different behavior that depends strongly on the spatial arrangement of impurities in the cluster.

*Unsteady shock-wave dynamics.* We now consider the time-dependent behavior preceding the formation of steady density distribution. Upon sudden application of a stream-inducing driving field, two oppositely directed (downstream and upstream) shock waves with kinklike profiles are formed and evolve away from an impurity cluster [see Figs. 3(a) and 3(b) for the case of a compact cluster (obstacle)]. This behavior is common for clusters of different types shown in Figs. 1(a)–1(e), in case they are large ( $R \gg \ell$ ) and dense enough to collectively provoke nonlinear density-coat formation (for the latter to come into effect, we also should remain within a certain range of values of bath fraction and driving field [35]). The compressionlike shock wave moving upstream reflects the growth dynamics of the dense region adjacent to the obstacle’s surface. The rarefactionlike one in the downstream region is responsible for the formation of a depleted tail or cavity (localization of vacancies). The overall stationary density profile represents the residual perturbation left after the stream scattering by impurities at  $t \rightarrow \infty$  (steady scattering state). The dynamics of the two shock waves is, generally, different but obeys the common inversion property upon switching from the  $n_0 < 0.5$  to the  $n_0 > 0.5$  domain [35].

*“Stopping effect”.* Let us first consider the formation of a dense compact region in front of a cluster, resulting from stopping the compression shock wave at  $n_0 < 0.5$ . For simplicity, we examine the behavior of the center-line profile which corresponds to the central region of the shock wave at  $y_i = 0$  [Figs. 3(a) and 3(b)] for the case of an impermeable circular obstacle. As can be seen from Fig. 3(a), the shock wave comes to a halt at certain standoff distance  $x_f^*$  ( $x_f$  is the front<sup>4</sup> position): once the condition  $n_f = n(x_f, 0) = 0.5$  is reached, the motion vanishes, i.e., shock-front speed  $v_f \rightarrow 0$ . This criterion holds also for nonregular clusters [see Fig. 1(f)]. The front speed asymptotically decays as  $v_f(t) \propto e^{-\gamma t}$ . The front speed of the downstream shock wave decays according to power law and does not undergo stopping, forming a depleted tail (for details, see [35]).

At  $n_0 > 0.5$ , there is no stopping effect for the upstream shock wave, while it does occur for the downstream wave.

<sup>1</sup>A similar effect of the strong local fluctuations of a scattered field appears for electromagnetic field scattering on fractal clusters of nanoparticles, so-called “hot spots” [32–34].

<sup>2</sup>Some properties of this interaction were previously considered for a pair of impurities in [2,6,8].

<sup>3</sup>We exploit the drag force definition  $\mathbf{f} = -\int_S \mathbf{n}(\mathbf{r}) \delta n(\mathbf{r}) d\mathbf{r}$ , where  $\mathbf{n}(\mathbf{r})$  is the exterior normal of inclusion surface  $S$  at the point  $\mathbf{r}$  (see [6–8]). For single-site inclusions we use a discretized version of this expression [17].

<sup>4</sup>Shock-front position  $x_f$  corresponds to the inflexion point of  $\langle n(x_i, y_i) \rangle|_{y_i=0}$ . As  $x_f$  takes discrete values, we use the smoothing procedure [35] for  $x_f(t)$  and  $v_f(t)$ .

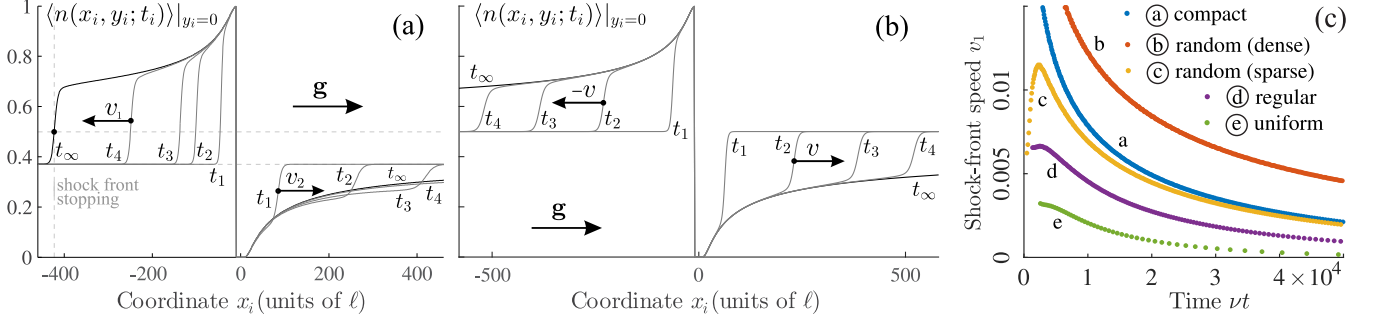


FIG. 3. Density profiles  $\langle n(x_i, y_i) \rangle|_{y_i=0}$  around an impermeable obstacle of radius  $R = 10.8\ell$  at the time moments  $t_1 < t_2 < t_3 < t_4$  and bath fractions (a)  $n_0 = 0.37$  and (b)  $n_0 = 0.5$ ;  $|\mathbf{g}| = 0.5$ . The lines at  $\nu t_\infty = 5 \times 10^4$  show the steady-state profiles established after long-time evolution; corresponding 2D density distribution for  $n_0 = 0.37$  (a) is shown in Fig. 1(a). (c) The time dependence of speed  $v_1$  [in units of  $\ell/(\nu t)$ ] of frontal shock waves propagation for clusters from Figs. 1(a)–1(e); lines are labeled to match Fig. 1.

Such “switching” is in agreement with the wake-inversion effect [8,18,35]. At  $n_0 = 0.5$ , both shock waves do not undergo stopping and decay asymptotically as  $n_f \propto 1/2 \pm At^{-\beta}$  [Fig. 3(b)].

Shock-front stopping criterion can be roughly estimated within the continual approximation [8,18]. A coarse description of the system is given by the Burgers-type equation that admits a kinklike solution. Far from the cluster, this equation takes the form  $\partial_t n = \nabla^2 n - (\mathbf{g} \cdot \nabla)[n(1-n)]$ . The growth of the blockade region (shock-front propagation) takes place when inflow of the gas particles prevails over their outflow via lateral diffusion. One may suppose that, for a large and dense impurity cluster, accumulation dynamics in the central region (center-line at  $y = 0$ ) can be approximately described by a quasi-one-dimensional (quasi-1D) equation. Its solution represents a kink approaching values  $n_-$ ,  $n_+$  as  $x \rightarrow \pm\infty$  and has the form  $n(x, t) = n_0 - \Delta n \tanh g \Delta n [x + v_f t - x_0]$ ,  $\Delta n = |n_- - n_+|/2$  is the shock half-height, and the speed of shock wave  $v_f$  is given by  $v_f = 2g(1/2 - n_f)$ , where  $n_f = (n_- + n_+)/2$ .<sup>5</sup> At  $n_f \rightarrow 0.5$ , the shock-front motion vanishes, i.e.,  $v_f \rightarrow 0$ . This stands for the quantitative stopping criterion which is in agreement with the numerical results for the center-line profile of shock wave in the 2D case [Figs. 3(a) and 1(f)]. The quasi-1D case allows one only to estimate the stopping condition and does not give a full description of the 2D shock wave, its lateral region, and asymptotic behaviors.

Now we consider the effects caused essentially by irregularity in the distribution of impurities. The first specific property is that the decomposition of a solid obstacle or homogeneous impurity cluster into an inhomogeneous cluster can result in the enhancement of shock wave—an increase in its amplitude and front speed [see Fig. 3(c) and corresponding steady-state profiles in Fig. 1]. The other property is what can be referred to as the precursor effect.

At the initial stage, just after abrupt application of the external drive, an impurity cluster is capable of generating larger density perturbation, both “stored” within a cluster and around it, than that held in a steady state. For this reason, the system tends to subsequently get rid of the excess

density perturbation that can be realized by the following two mechanisms:

(i) The excessive portion of density perturbation “leaves” the cluster in the form of a solitary wave traveling downstream<sup>6</sup> at  $n_0 < 0.5$  [Fig. 4(a)] or upstream at  $n_0 > 0.5$  [Figs. 4(b) or 4(c)], which is in accordance with the wake inversion effect

<sup>6</sup>This recalls the avalanche problem for a pile of sand [36].

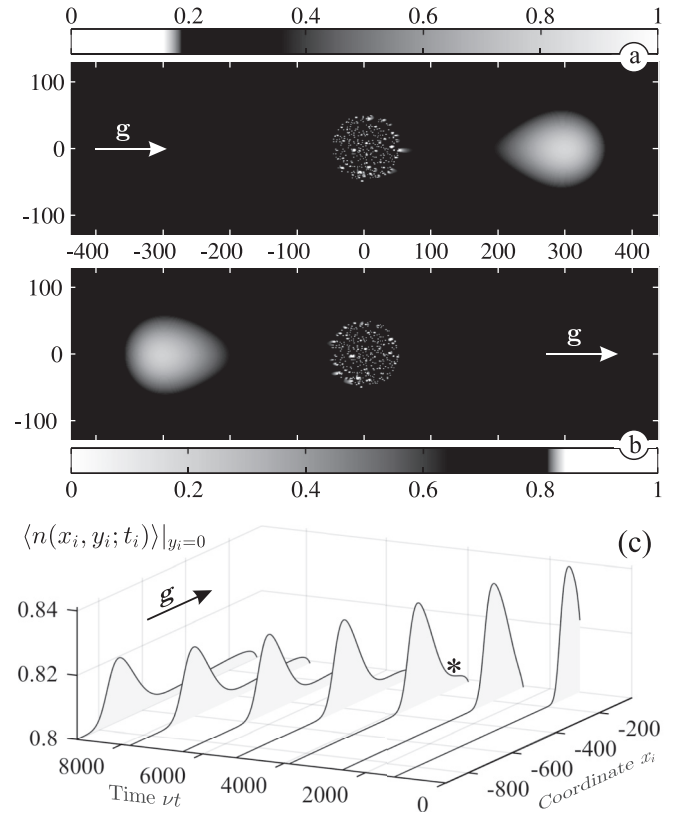


FIG. 4. Momentary gas distributions  $|\delta n(x_i, y_i)|$  at  $\nu t = 3.9 \times 10^3$  illustrating the precursor propagation: bunch of gas particles (b) or holes (a) separating from the impurity cluster. (c) The time evolution of density profile  $\delta n(x_i, \nu t; y_i = 0)$ ; the profile marked by an asterisk corresponds to panel (b). Cluster density  $\phi = 0.0461$ ,  $n_0 = 0.2$  for (a),  $n_0 = 0.8$  for (b) and (c),  $|\mathbf{g}| = 0.5$ .

<sup>5</sup> $n_\pm \approx n(x_f \pm \Delta)$  can be associated with shock height;  $\Delta$  is the shock-front thickness.

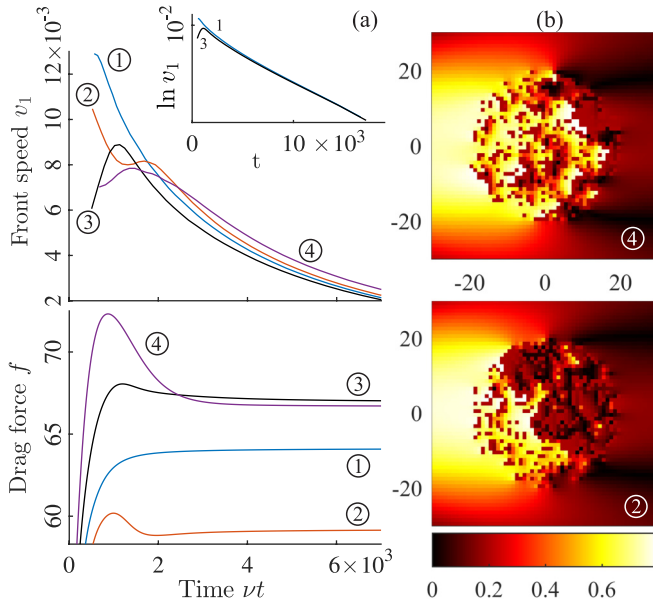


FIG. 5. Time dependence of the shock-front speed and total drag force (a) for several realizations 1–4 of a random impurity cluster.  $N = 362$ ,  $R = 20\ell$ ,  $|\mathbf{g}| = 0.5$ ,  $n_0 = 0.2$ ;  $f$  and  $v_1$  are in units of  $kT/l$  and  $\ell/(\nu t)$ , correspondingly. The front speed slowdown is nearly exponential,  $\ln v_1 \propto -t$  [see the inset in (a)]. (b) Steady-state distributions of  $\delta n^2(x_i, y_i)$  within a cluster, realizations 4, 2.

[18]. The “ejected” bunch of gas particles (or vacancies) and associated hump-shaped wave (or the inverse hump) have a characteristic length scale (its half-width) commensurate with the cluster size  $2R$ . This precursorlike mechanism takes place for sparse clusters,  $\phi \ll 1$ , for which the common blockade region ahead of scatterers is either weak or not formed.

(ii) A different mechanism comes into play for modestly dense clusters, when the excessive perturbation is relaxed via temporal acceleration of the shock front at the initial times. It can be explained by considering the dynamic behavior for several realizations of random cluster with an intermediate value of fraction  $\phi \approx 10^{-1}$  [see Fig. 5]. As Fig. 5(a) suggests, shock-front speed acceleration is sensitive to the realizations of random cluster. This temporal acceleration is always preceded with or accompanied by the enhancement peak of total drag force [Fig. 5(b)], while for the cluster realization without acceleration effect the drag force exhibits monotonic saturation. The temporal force enhancement signifies the presence of excess

perturbation (within a cluster) that subsequently transfers into shock-wave acceleration. Under sudden stream activation, the nonlinear blockade effect leads to local saturation of scalar density field  $n(\mathbf{r}, t)$  attained faster than the overall perturbation is redistributed to minimize the total drag force. This leads to the accelerated growth of the blockade region at the initial times.

Note, system behavior is also sensitive to the variables of gas flow: bath fraction  $n_0$  and magnitude of driving force  $\mathbf{G}$ . The shock-front stopping property is consistent with the concentration-dependent wake-inversion effect of [18]. In the domain  $n_0 < 0.5$ , the increase of  $n_0$  and/or  $\mathbf{G}$  leads to the enhancement of scattering and shock wave, while the qualitative picture of scattering is not changed; so, we give details on this study in the Supplemental Material [35].

*Concluding remarks.* We presented some results on the effects of collective scattering of a gas stream on finite-sized impurity clouds and associated shock-wave generation, both accompanied by a nonlinear blockade effect. Based on a numerical solution of kinetic equations for the average local occupation numbers of lattice gas, we display the significant role of spatial disorder of scatterers (impurities). Our results show that scattering of gas flow on impurity cloud and shock-wave generation can be enhanced by decomposition of a solid obstacle into fragments or a sparse cluster of impurities. This enhancement is more efficient for disordered clusters as compared to regular ones. Note that the shock-wave amplification effect correlates, to a certain extent, with the well-known problem of air shock-wave interaction with a porous screen where the effect of temporal enhancement of a reflected shock wave was observed [37,38]. In addition, a disordered cluster of scatterers can provoke high local fluctuations of a scattered field inside the cluster and an avalanchelike effect at a sudden application of the external driving field. The considered effects reveal a close formal analogy to the classical problem of light scattering in atomic, molecular, or nanoparticle ensembles.

The simplest hard-core lattice gas model alone leads to the peculiar nonlinear effects mentioned above, which can be of interest considering the kinetics of adatoms on solid surfaces [24], surface electromigration [39], or superionic conductors [22]. Further application of more realistic Coulomb, Yukawa, or Lennard-Jones potentials of interparticle interaction, can better describe particular physical systems, e.g., dusty plasmas or colloidal dispersions (see [20,40–42]).

*Acknowledgments.* We are grateful to V. V. Gozhenko, Professor B. I. Lev, and E. V. Stolyarov for their attention to this work.

[1] G. Birkhoff and E. H. Zarantonello, *Jets, Wakes, and Cavities* (Academic, London, 1957).  
 [2] A. S. Khair and J. F. Brady, *Proc. R. Soc. A* **463**, 223 (2007).  
 [3] J. Bartnick, A. Kaiser, H. Löwen, and A. V. Ivlev, *J. Chem. Phys.* **144**, 224901 (2016).  
 [4] D. Pines and P. Nozières, *The Theory of Quantum Liquids, V. 1: Normal Fermi Liquids* (W. A. Benjamin, New York, 1966).

[5] A. M. Kamchatnov and L. P. Pitaevskii, *Phys. Rev. Lett.* **100**, 160402 (2008).  
 [6] J. Dzubiella, H. Löwen, and C. N. Likos, *Phys. Rev. Lett.* **91**, 248301 (2003); R. Wulfert, U. Seifert, and T. Speck, *Soft Matter* **13**, 9093 (2017).  
 [7] K. Hayashi and S. Sasa, *J. Phys.: Condens. Matter* **18**, 2825 (2006).

- [8] O. V. Kliushnychenko and S. P. Lukyanets, *Phys. Rev. E* **95**, 012150 (2017).
- [9] M. J. Pinheiro, *Phys. Scr.* **84**, 055004 (2011).
- [10] E. A. Lisin, O. S. Vaulina, and O. F. Petrov, *J. Exp. Theor. Phys.* **124**, 678 (2017).
- [11] A. V. Ivlev, J. Bartnick, M. Heinen, C.-R. Du, V. Nosenko, and H. Löwen, *Phys. Rev. X* **5**, 011035 (2015).
- [12] M. Durve, A. Saha, and A. Sayeed, *Eur. Phys. J. E* **41**, 49 (2018).
- [13] O. V. Kliushnychenko and S. P. Lukyanets, *Eur. Phys. J.: Spec. Top.* **216**, 127 (2013).
- [14] D. Frydel and H. Diamant, *Phys. Rev. Lett.* **104**, 248302 (2010).
- [15] B. U. Felderhof, *J. Chem. Phys.* **134**, 024505 (2011).
- [16] S. Leitmann, T. Schwab, and T. Franosch, *Phys. Rev. E* **97**, 022101 (2018); S. Leitmann and T. Franosch, *Phys. Rev. Lett.* **118**, 018001 (2017).
- [17] C. Mejía-Monasterio and G. Oshanin, *Soft Matter* **7**, 993 (2011).
- [18] O. V. Kliushnychenko and S. P. Lukyanets, *J. Exp. Theor. Phys.* **118**, 976 (2014).
- [19] O. Bénichou, P. Illien, G. Oshanin, A. Sarracino, and R. Voituriez, *Phys. Rev. E* **93**, 032128 (2016).
- [20] O. A. Vasilyev, O. Bénichou, C. Mejía-Monasterio, E. R. Weeks, and G. Oshanin, *Soft Matter* **13**, 7617 (2017).
- [21] A. Poncet, O. Bénichou, V. Démary, and G. Oshanin, *Phys. Rev. Lett.* **118**, 118002 (2017).
- [22] B. Schmittmann and R. K. P. Zia, *Statistical Mechanics of Driven Diffusive Systems* (Academic, London, 1995).
- [23] R. A. Tahir-Kheli and R. J. Elliott, *Phys. Rev. B* **27**, 844 (1983).
- [24] A. A. Chumak and A. A. Tarasenko, *Surf. Sci.* **91**, 694 (1980).
- [25] K.-T. Leung, *Phys. Rev. Lett.* **73**, 2386 (1994).
- [26] S. P. Lukyanets and O. V. Kliushnychenko, *Phys. Rev. E* **82**, 051111 (2010).
- [27] M. von Smoluchowski, *Ann. Phys.* **330**, 205 (1908).
- [28] Y. L. Klimontovich and V. S. Fursov, *Zh. Eksp. Teor. Fiz.* **19**, 819 (1949).
- [29] V. A. Alekseev, A. V. Vinogradov, and I. I. Sobel'man, *Sov. Phys. Usp.* **13**, 576 (1971).
- [30] Y. L. Klimontovich, *Kinetic Theory of Electromagnetic Processes* (Springer, Berlin, 1983).
- [31] I. I. Sobel'man, *Phys. Usp.* **45**, 75 (2002).
- [32] M. I. Stockman, S. V. Faleev, and D. J. Bergman, *Phys. Rev. Lett.* **87**, 167401 (2001).
- [33] M. I. Stockman, *Physics* **3**, 90 (2010).
- [34] A. K. Sarychev, V. A. Shubin, and V. M. Shalaev, *Phys. Rev. E* **59**, 7239 (1999).
- [35] See Supplemental Material at <http://link.aps.org/supplemental/10.1103/PhysRevE.98.020101> for additional data on collective scattering in the extended range of values of flow variables and some complementary parametric dependencies, concerning inversion property and front dynamics.
- [36] P. Bak, *How Nature Works: The Science of Self-Organised Criticality* (Copernicus, New York, 1996).
- [37] B. E. Gel'fand, S. A. Gubin, S. M. Kogarko, and O. E. Popov, *J. Appl. Mech. Tech. Phys.* **16**, 897 (1975).
- [38] B. E. Gel'fand, A. V. Gubanov, and E. I. Timofeev, *Fluid Dyn.* **18**, 561 (1983).
- [39] M. Schimschak and J. Krug, *Phys. Rev. Lett.* **78**, 278 (1997).
- [40] V. N. Tsytovich and N. G. Gusein-zade, *Plasma Phys. Rep.* **39**, 515 (2013).
- [41] V. N. Tsytovich, *Phys. Usp.* **58**, 150 (2015).
- [42] I. Sriram and E. M. Furst, *Soft Matter* **8**, 3335 (2012); *Phys. Rev. E* **91**, 042303 (2015).